Adsorption Hysteresis of Nitrogen and Argon in Pore Networks and Characterization of Novel Micro- and Mesoporous Silicas

Matthias Thommes,*,† Bernd Smarsly,‡ Matthijs Groenewolt,‡ Peter I. Ravikovitch,§ and Alexander V. Neimark*,§

Quantachrome Instruments, 1900 Corporate Drive, Boynton Beach, Florida 33426, Max-Planck Institute of Colloids and Interfaces, D-14424, Potsdam, Germany, and Center for Modeling and Characterization of Nanoporous Materials, TRI/ Princeton, 601 Prospect Avenue, Princeton, New Jersey 08540-0625

Received June 22, 2005. In Final Form: October 20, 2005

We report results of nitrogen and argon adsorption experiments performed at 77.4 and 87.3 K on novel micro/mesoporous silica materials with morphologically different networks of mesopores embedded into microporous matrixes: SE3030 silica with wormlike cylindrical channels of mode diameter of ∼95 Å, KLE silica with cagelike spheroidal pores of ca. 140 Å, KLE/IL silica with spheroidal pores of ∼140 Å connected by cylindrical channels of ∼26 Å, and, also for a comparison, on Vycor glass with a disordered network of pores of mode diameter of ∼70 Å. We show that the type of hysteresis loop formed by adsorption/desorption isotherms is determined by different mechanisms of condensation and evaporation and depends upon the shape and size of pores. We demonstrate that adsorption experiments performed with different adsorptives allow for detecting and separating the effects of pore blocking/percolation and cavitation in the course of evaporation. The results confirm that cavitation-controlled evaporation occurs in ink-bottle pores with the neck size smaller than a certain critical value. In this case, the pressure of evaporation does not depend upon the neck size. In pores with larger necks, percolation-controlled evaporation occurs, as observed for nitrogen (at 77.4 K) and argon (at 87.3 K) on porous Vycor glass. We elaborate a novel hybrid nonlocal density functional theory (NLDFT) method for calculations of pore size distributions from adsorption isotherms in the entire range of micro- and mesopores. The NLDFT method, applied to the adsorption branch of the isotherm, takes into account the effect of delayed capillary condensation in pores of different geometries. The pore size data obtained by the NLDFT method for SE3030, KLE, and KLE/IL silicas agree with the data of SANS/SAXS techniques.

1. Introduction

Pore size analysis of mesoporous materials from adsorption isotherms is based on an adopted interpretation of the mechanisms of capillary condensation and evaporation and associated hysteresis phenomena (refs 1 and 2 and references therein). Two principal factors determine the hysteretic behavior: hysteresis on the level of a single pore of a given shape and cooperative effects reflecting the specifics of connectivity of the pore network. On the pore level, adsorption hysteresis is considered as an intrinsic property of the vapor−liquid-phase transition in a finite volume system. A classical scenario of capillary condensation implies that the vapor−liquid transition is delayed because of the existence of metastable adsorption films and hindered nucleation of liquid bridges.[3−9] The nonlocal density functional theory (NLDFT) models revealed that, in principle, both condensation and evaporation can be associated with metastable states of the pore fluid.[6,8,9] This is consistent with the classical van der Waals theory,[8c] which predicts that the metastable adsorption branch terminates at a vaporlike spinodal that corresponds to the limit of stability for the metastable adsorbed films. Accordingly, the metastable desorption branch terminates at a liquidlike spinodal, which corresponds to the limit of stability of metastable (stretched) condensed fluid. In open uniform cylindrical pores, however, metastabilities occur only on the adsorption branch. Indeed, in an open pore filled by liquidlike condensate, the liquid−vapor interface is already present and evaporation occurs without nucleation, via a receding meniscus. That is, the desorption process is associated with the equilibrium vapor−liquid transition, whereas the condensation process involves nucleation of liquid bridges. In sufficiently wide pores, the barrier in the nucleation process is too high and condensation occurs spontaneously near the vaporlike spinodal.

This mechanism of adsorption hysteresis is dominant in ordered mesoporous materials with uniform cylindrical pores such as MCM-41 and SBA-15. Typically, one observes a hysteresis loop of type H1, according to the IUPAC classification, with parallel adsorption and desorption branches. The NLDFT method relates the location of the vaporlike spinodal with the pore size.[9] It is assumed that spontaneous condensation occurs at the spinodal. The kernel of NLDFT metastable adsorption isotherms can be used to obtain the pore size distribution from the adsorption branch of the isotherm. If hysteresis is caused solely by the

* To whom correspondence should be addressed. E-mail: matthias.thommes@quantachrome.com (M.T.). E-mail: aneimark@triprinceton.org (A.V.N.).

† Quantachrome Instruments.

‡ Max-Planck Institute of Colloids and Interfaces.

§ Center for Modeling and Characterization of Nanoporous Materials.

(1) Sing, K. S. W.; Everett, D. H.; Haul, R. A. W.; Mouscou, L.; Pierotti, R. A.; Rouquerol, J.; Siemieniewska, T. *Pure Appl. Chem.* **1985**, *57*, 603.

(2) Thommes, M. In *Nanoporous Materials: Science and Engineering*; Lu, G. Q.; Zhao, X. S.; Eds.; Imperial College Press: London, U.K., 2004; pp 317−364.

(3) Everett, D. H. In *The Solid−Gas Interface*; Flood, E. A.; Ed.; Decker: New York, 1967; Vol. 2, pp 1055−1113.

(4) Cole, M. W.; Saam, W. F. *Phys. Rev. Lett.* **1974**, *32*, 985.

(5) Awschalom, D. D.; Warnock, J.; Shafer, M. W. *Phys. Rev. Lett.* **1996**, *57*, 1607.

(6) (a) Ball, P. C.; Evans, R. *Langmuir* **1989**, *5*, 714. (b) Evans, R. *J. Phys.: Condens. Matter* **1990**, *2*, 8989.

(7) Ravikovitch, P. I.; Domhnaill, S. C. O.; Neimark, A. V.; Schueth, F.; Unger, K. K. *Langmuir* **1995**, *11*, 4765.

(8) (a) Neimark, A. V.; Ravikovitch, P. I.; Vishnyakov, A. *Phys. Rev. E* **2000**, *62*, R1493. (b) Vishnyakov, A.; Neimark, A. V. *J. Chem. Phys.* **2003**, *119*, 9755. (c) Neimark, A. V.; Ravikovitch, P. I.; Vishnyakov, A. *J. Phys.: Condens. Matter* **2003**, *15*, 347.

(9) (a) Neimark, A. V.; Ravikovitch, P. I. *Microporous Mesoporous Mater.* **2001**, *44*, 697. (b) Ravikovitch, P. I.; Neimark, A. V. *Colloids Surf., A* **2001**, *187*, 11.

10.1021/la051686h CCC: $33.50 © 2006 American Chemical Society
Published on Web 12/15/2005

delayed condensation effect, pore sizes calculated from the adsorption branch (by applying the kernel of metastable adsorption isotherms) and pore sizes calculated from the desorption branch (by applying the kernel of equilibrium isotherms) must be consistent. This consistency was found for MCM-41, SBA-15,[2,8a] and for CPG (controlled pore glass) silica samples.[2]

To describe hysteresis phenomena in disordered adsorbents, the network models have been developed (e.g., refs 10−15).[10−15] The network models attribute hysteresis to the so-called *pore blocking* or percolation effect. This effect is expected to occur if the pore has access to the external surface only through a narrower neck, as in the ink-bottle pore.[16−18] The wide body of the ink-bottle pore is filled at the vapor pressure, which corresponds to delayed condensation, and remains filled during desorption until the narrow neck empties first at a lower vapor pressure. Thus, in a network of ink-bottle pores, evaporation of the capillary condensate is obstructed by the pore necks. The vapor pressure, at which a pore body empties, depends upon the size of the necks, the connectivity of the network, and the state of the neighboring pores. The pore network empties when the relative pressure is below a characteristic percolation threshold associated with the onset of a continuous cluster of pores open to the surface.[11−13] In such a case, the desorption branch of the hysteresis loop is significantly steeper than the adsorption branch, which results in a triangular hysteresis loop of type H2 according to the IUPAC classification. For example, it is believed that the observed type H2 hysteresis in porous Vycor glass is associated with the occurrence of percolation effects (e.g., ref 19). Capillary condensation hysteresis in disordered systems and effects caused by correlations between pores have recently been studied using both molecular[20,21] and lattice models.[22,23]

Adsorption/desorption mechanisms in ink-bottle-type pores were recently revisited.[24−27] In particular, theoretical,[25a] molecular simulation,[26] and experimental[25b,28] studies, which employed novel mesoporous materials consisting of well-defined ink-bottle pores, such as FDU-1,[29] PHTS,[28] and SBA-16,[29b,30−32] revealed that, if the neck diameter is smaller than a certain critical size

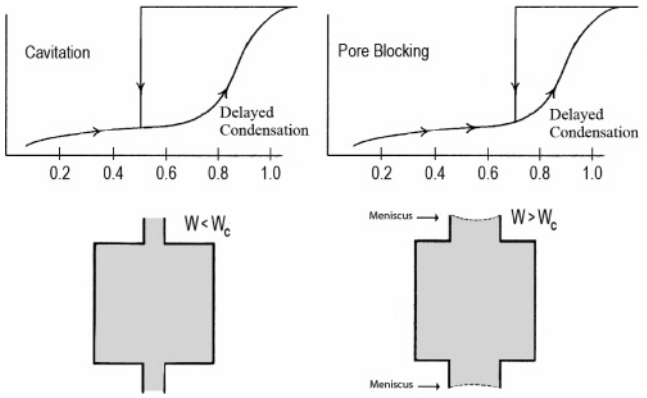

Figure 1. Schematic illustration of pore blocking and cavitation phenomena.

at a given experimental temperature, desorption from the pore body occurs via *cavitation* (spontaneous nucleation of a bubble). In this case, desorption occurs at a pressure P_{cav}, which is higher than the pressure of equilibrium evaporation from the pore neck P_{neck}. The pore body can empty by diffusion. while the pore neck remains filled.[24,26] Classical pore-blocking effect takes place when the neck size is greater than a certain characteristic value (ca. 50 Å for nitrogen at 77.4 K, assuming that the neck can be considered as a cylindrical pore[25b]).

The cavitation effect was correlated with the lower limit of hysteresis of the desorption isotherm, which is traditionally discussed within the framework of the tensile strength hypothesis.[32−36] In this classical approach, which dates back to the works of Schofield, Kadlec and Dubinin, and Burgess and Everett,[32−36] it was supposed that the tensile stress limit of condensed fluid, which is indicated by cavitation, does not depend upon the nature and the pore structure of the adsorbent yet is a universal feature of the adsorptive. This conclusion was supported by the fact that, in many mesoporous systems, the lower closure point of the hysteresis loop was observed in a very narrow range of relative pressures, about 0.42 for nitrogen at 77.4 K, ∼0.25 for argon at 77.4 K, and ∼0.38 for argon at 87.3 K. Noteworthy, these "universal" values correlate with the characteristic pressure of the disappearance of hysteresis in MCM-41 and SBA-15 materials, which contain cylindrical pore channels. However, the cavitation-induced stepwise desorption in the ink-bottle pores of FDU-1 and SBA-16 mesoporous molecular sieves[25] occurs at appreciably larger pressures (∼$0.055P_0$ larger) than the "universal" lower closure point of hysteresis mentioned above. The authors[25] concluded that the cavitation pressure and, respectively, the lower closure point of hysteresis may depend upon the pore geometry, i.e., upon pore size and shape. Further, the authors[31] presented a correlation between the desorption pressure and condensation pressure, which relates to the pore size.

For given adsorptive and temperature, the neck diameter of an ink-bottle pore determines the mechanism of evaporation from the pore body. This situation is illustrated schematically in Figure 1. In the case of pore blocking, the evaporation occurs at the pressure of equilibrium meniscus in the pore neck, and information

(10) Mason, G. *J. Colloid Interface Sci.* **1982**, *88*, 36.
(11) Wall, G. C.; Brown, R. J. C. *J. Colloid Interface Sci.* **1981**, *82*, 141.
(12) (a) Neimark, A. V. *Rep. Acad. Sci. USSR (Phys. Chem.)* **1983**, *273*, 867. (b) Neimark, A. V. *Colloid J.* **1986**, *46*, 1004.
(13) Parlar, M.; Yortsos, Y. *J. Colloid Interface Sci.* **1988**, *124*, 162.
(14) Zhu, H.; Zhang, L.; Seaton, N. A. *Langmuir* **1993**, *9*, 2576.
(15) Cordero, S.; Kornhauser, I.; Dominguez, A.; Felipe, C.; Marcos, E. J.; Rojas, F.; Lopez, R. H.; Vidales, A. M.; Riccardo, J. L.; Zgrablich, G. *Part. Part. Syst. Charact.* **2004**, *101*, 116.
(16) Kraemer, E. O. In *Treatise on Physical Chemistry*, D. van Nostrand: New York, 1931.
(17) McBain, J. W. *J. Am. Chem. Soc.* **1935**, *57*, 699.
(18) Gregg, S. J.; Sing, K. S. W. In *Adsorption, Surface Area, and Porosity*, Academic Press: London, U.K., 1982.
(19) Page, J. H.; Liu, L.; Abeles, B.; Herbolzheimer, E.; Deckmann, H. W.; Weitz, D. A. *Phys. Rev. E* **1995**, *52*, 2763.
(20) Page, K. S.; Monson, P. A. *Phys. Rev. E* **1996**, *54*, 6557.
(21) Gelb, L. D.; Gubbins, K. E. *Langmuir* **1998**, *14*, 2097.
(22) Kierlik, E.; Rosinberg, M. L.; Tarjus, G.; Viot, P. *Phys. Chem. Chem. Phys.* **2001**, *3*, 1201.
(23) Woo, H. J.; Sarkisov, L.; Monson, P. A. *Langmuir* **2001**, *17*, 7472.
(24) Sarkisov, L.; Monson, P. A. *Langmuir* **2001**, *17*, 7600.
(25) (a) Ravikovitch, P. I.; Neimark, A. V. *Langmuir* **2002**, *18*, 1550. (b) Ravikovitch, P. I.; Neimark, A. V. *Langmuir* **2002**, *18*, 9830.
(26) Vishnyakov, A.; Neimark, A. V. *Langmuir* **2003**, *19*, 3240.
(27) Libby, B.; Monson, P. *Langmuir* **2004**, *20*, 6482.
(28) van der Voort, P.; Ravikovitch, P. I.; De Jong, K. P.; Neimark, A. V.; Janssen, A. H.; Benjelloun, M.; van Bavel, E.; Cool, P.; Weckhuysen, B. M.; Vansant, E. F. *Chem. Commun.* **2002**, 1010.
(29) (a) Yu, C.; Yu, Y.; Zhao, D. *Chem. Commun.* **2000**, 575. (b) Kruk, M.; Antochshuk, V.; Matos, J. R.; Mercuri, L. P.; Jaroniec, M. *J. Am. Chem. Soc.* **2002**, *124*, 768.
(30) Morishige, K.; Tateishi, N. *J. Chem. Phys.* **2003**, *119*, 2301.
(31) Kim, T.-W.; Ryoo, R.; Kruk, M.; Gierszal, K. P.; Jaroniec, M.; Kamyia, S.; Terasaki, O. *J. Phys. Chem. B* **2004**, *108*, 11480.
(32) Schreiber, A.; Reinhardt, S.; Findenegg, G. H. *Stud. Surf. Sci. Catal.* **2002**, *144*, 177.
(33) (a) Schofield, R. K. *Discuss. Faraday Soc.* **1948**, *3*, 105. (b) Kadlec, O.; Dubinin, M. M. *J. Colloid Interface Sci.* **1969**, *31*, 479. (c) Burgess, C. G. V.; Everett, D. H. *J. Colloid Interface Sci.* **1970**, *33*, 611.
(34) Sonwane, C. G.; Bhatia, S. K. *Langmuir* **1999**, *15*, 5347.
(35) Di Renzo, F.; Galarneau, A.; Trens, P.; Tanchoux, N.; Fajula, F. *Stud. Surf. Sci. Catal.* **2002**, *142*, 142.
(36) Groen, J. C.; Peffer, L. A. A.; Perez-Ramirez, J. *Microporous Mesoporous Mater.* **2003**, *60*, 1.

about the neck size can be obtained from the desorption branch of the isotherm. In the case of cavitation, the evaporation pressure is not related to the size of the neck, and no information about the neck size can be obtained from the analysis of the desorption branch. Determination of the neck size is crucial for a comprehensive pore structure characterization. In principle, neck sizes in ordered materials with cagelike pore structures (e.g., SBA-1, SBA-6, and SBA-16) can be determined by high-resolution electron crystallography.[37] However, interpretation of the electron-potential maps requires a choice of a certain threshold value to define a pore boundary. In the systems with microporous walls, this procedure is complicated.[31] It was also suggested to determine the entrance sizes by postsynthesis surface modification by employing the reaction of the pore wall surface with a series of monofunctional organosilances of gradually increasing ligand sizes in combination with gas adsorption.[29b,31] Studies of the temperature dependence of the hysteresis loop in ink-bottle pores showed a transition between cavitation and pore-blocking regimes, which suggests a possibility of estimating the neck size distribution from the desorption isotherm by tuning the experimental conditions.[25b] For example, argon adsorption at 77.4 K allows the probing of the neck sizes down to 40 Å, and krypton adsorption at 87.3 K allows to probe the pore necks as small as ca. 30 Å.

In this work, we study adsorption behavior of nitrogen and argon at 77.4 and 87.3 K in novel ordered micro- and mesoporous silica materials (SE3030 silica,[38,41] KLE silica,[39] and KLE/IL silica) with morphologically different networks of mesopores embedded into microporous matrixes. We also invoke Vycor glass with a wide pore size distribution. We show that the use of different adsorptives allows one to identify and separate percolation and cavitation phenomena. A novel hybrid NLDFT method is applied to the adsorption branch of the hysteretic isotherms over a wide range of relative pressures to calculate micro- and mesopore size distributions. The NLDFT calculations are shown to agree with independent pore structure data of small-angle neutron scattering (SANS) and small-angle X-ray scattering (SAXS) techniques.

2. Materials and Methods

2.1. Materials. *SE3030 Silica.* The synthesis of SE3030 silica is described in ref 38. Lyotropic amphiphilic copolymer phases of poly(styrene)-block-poly(ethyleneoxide)-(SE) were used here as structure-directing agents. An accurate characterization of this material was provided by novel SANS[38,41] and SAXS methods, as well as transmission electronic microscopy (TEM) analysis. It was found from SANS analysis using the hard-disk model of Rosenfeld (for details, see ref 41) that the pore system can be considered as elongated wormlike mesopores (of ca. 95 Å in diameter) connected by narrow cylindrical micropores (i.e., the micropores of diameter ca. 1 nm are located in the pore walls, which have a thickness of ca. 6 nm).

KLE Silica. KLE silica contains mesopores of almost ideal spherical shape, which are arranged on a distorted FCC lattice.[39] In aqueous solution, the KLE block copolymer forms an FCC lattice of isolated spherical micelles. However, in KLE silica, the spherical KLE mesopores are connected through small micropores, originating from the hydrophilic poly(ethylene oxide) block penetrating the silica matrix. Thus, this cubic structure of spherical mesopores represents an ideal morphology to study the adsorption and desorption phenomena in pores of well-defined shape. A decrease in the polymer concentration in the initial starting solution can lead to isolation of KLE micelles, so that the polymer cannot be removed by calcination. The pore structure of KLE silica as confirmed by SAXS and TEM studies (for details, see ref 39) can be described as spherical mesopores of ca. 140 Å, in diameter connected via narrow (ca. 13 Å) cylindrical-like micropores in the pore walls.

KLE/IL Silica. KLE/IL silica is synthesized using the same block copolymer as KLE silica, but in addition, an "ionic liquid" is used as a second template.[40] This leads to a material that exhibits a trimodal pore size distribution: similarly to KLE silica, KLE/IL silica contains micropores of ca. 13 Å in diameter and main mesoporous cavities of spherical geometry and size of 138 Å, but in addition, these cavities are connected through narrow cylindrical mesopores of ca. 26 Å in diameter (from the ionic liquid). TEM images of KLE/IL silica were taken with a Zeiss EM 912Ω. SAXS patterns were recorded using a Cu Kα rotating anode instrument.[40] The original formula used for KLE silica and KLE/IL silica[39] was optimized (see ref 40) to improve accessibility of the mesopores.

Vycor Glass. Porous Vycor glass (Corning 7930) was obtained from Corning (via Advanced Glass and Ceramics, Holden, MA).

2.2. High-Resolution Adsorption Measurements. Nitrogen (77.4 K) and argon (77.4 and 87.3 K) adsorption/desorption measurements were performed with an Autosorb-I-MP instrument (Quantachrome Instruments, Boynton Beach, FL) in the relative pressure range P/P_0 from 1×10^{-6} to 1. The analysis station of the volumetric adsorption apparatus was equipped, in addition to the standard pressure transducers in the dosing volume (manifold) of the apparatus, with high-precision pressure transducers (Baratron MKS) dedicated to read the pressure in the sample cell itself. Hence, the sample cell was isolated during equilibration that ensured a very small effective dead volume and therefore a highly accurate determination of the adsorbed amount. To provide high accuracy and precision in the determination of P/P_0, the saturation pressure P_0 was measured throughout the entire analysis by means of a dedicated saturation pressure transducer, which allowed us to monitor the vapor pressure for each data point. The samples were outgassed overnight at 150 °C prior to the adsorption analysis.

2.3. NLDFT Method for Pore Size Characterization. The adsorption data were analyzed using a novel hybrid NLDFT approach that allows quantification of both micro- and mesopores. The NLDFT method, which has been previously shown to give quantitatively correct pore size distributions in silica materials with cylindrical[9] and spherical[25a] mesopores, has been extended to the range of micropores, i.e. down to 5 Å pores. A new hybrid approach has been used to calculate pore size distributions in micro- and mesoporous silicas containing pores of different geometry. For materials with cylindrical mesopores (e.g., SE3030 silica), the method uses a cylindrical pore model for both meso- and micropores. For materials with cagelike mesopores (e.g., KLE and KLE/IL silicas), the method uses a spherical pore model in the region of pores that exhibits adsorption/desorption hysteresis and a cylindrical pore model in the region of reversible filling of micropores and small mesopores. Thus, the method allows one to calculate pore size distributions in the complete range of micro- and mesopores from the adsorption branch of the isotherm. In the region of hysteresis, the method takes into account the effect of delayed condensation and uses NLDFT metastable adsorption isotherms, while in the region of reversible capillary condensation/desorption, the method uses NLDFT equilibrium isotherms.

3. Results and Discussion

3.1. Adsorption Isotherms and Pore Size Characterization. A Comparison with SANS/SAXS. High-resolution nitrogen (77.4 K) and argon (87.3 K) adsorption/desorption isotherms on SE3030, KLE, and KLE/IL silica are shown in Figures 2a, 3a, and 4a. Semilogarithmic plots, emphasizing the low relative

(37) Sakamoto, Y.; Kaneda, M.; Terasaki, O.; Zhao, D. Y.; Kim, J. M.; Stucky, G. D.; Shin, H. J.; Ryoo, R. *Nature* **2000**, *408*, 449.
(38) Smarsly, B.; Goeltner, C.; Antonietti, M.; Ruland, W.; Hoinkis, E. *J. Phys. Chem. B* **2001**, *105*, 831.
(39) Thomas, A.; Schlaad, H.; Smarsly, B.; Antonietti, M. *Langmuir* **2003**, *19*, 4455.
(40) Kuang, D.; Smarsly, B.; Brezesinski, T. *J. Am. Chem. Soc.* **2004**, *126*, 10534.
(41) Smarsly, B.; Thommes, M.; Ravikovitch, P. I.; Neimark, A. V. *Adsorption* 2005, *11*, 653.

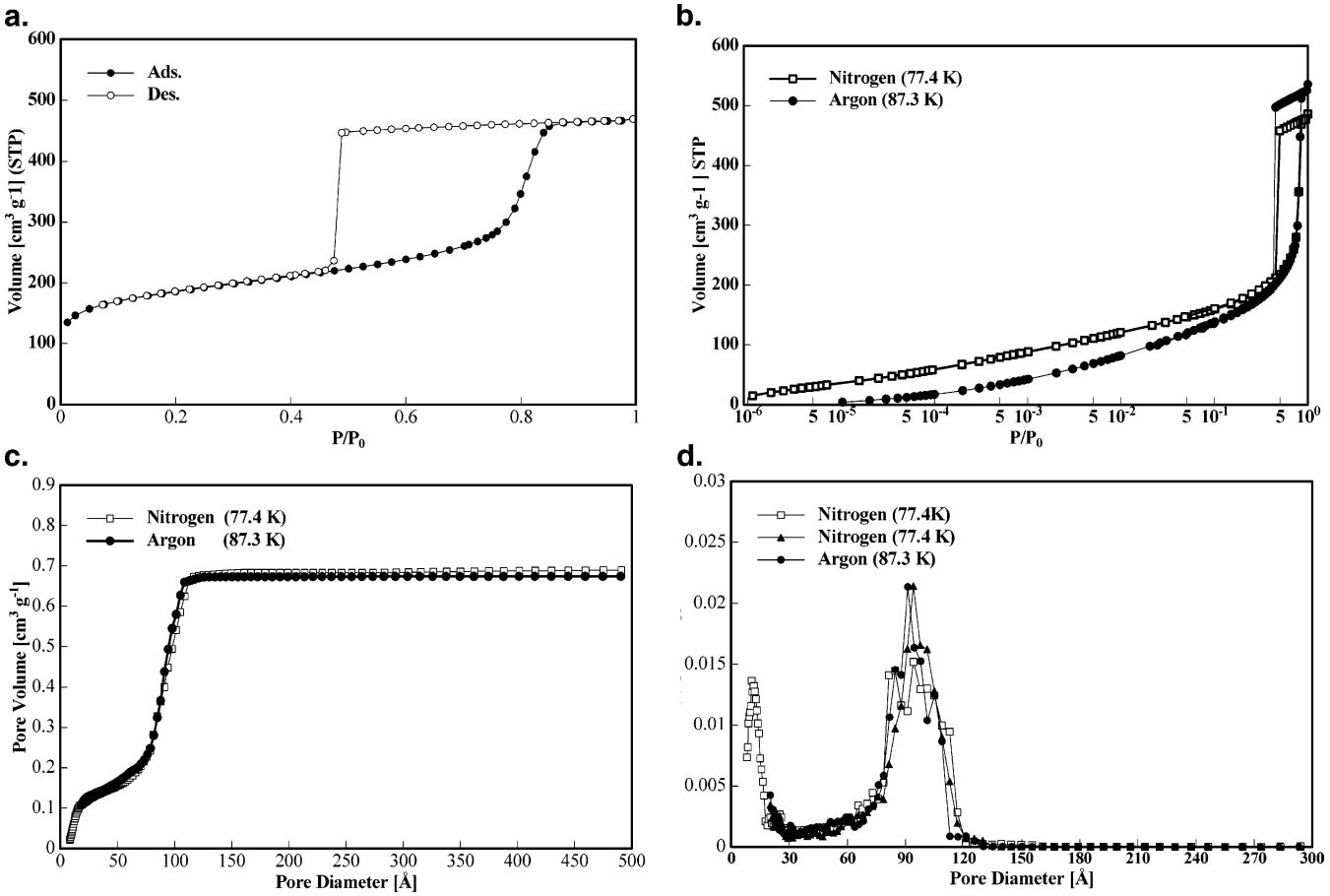

Figure 2. (a) High-resolution nitrogen (77.4 K) adsorption/desorption isotherm on SE3030 silica. (b) Nitrogen (77.4 K) and argon (87.3 K) adsorption/desorption on SE3030 silica (semilogarithmic plot). (c) NLDFT cumulative pore volume plots calculated from the adsorption branch of the adsorption/desorption isotherms shown in b by applying the kernel of metastable adsorption isotherms based on a cylindrical pore model for the systems nitrogen (77.4 K)/silica and argon (87.3 K)/silica. (d) NLDFT differential pore size distribution for SE3030 silica from nitrogen (77.4 K) and argon (87.3 K) adsorption data (see b and c).

pressure region of the isotherms on SE3030 and KLE/IL silicas, are presented in Figures 2b and 4b. All isotherms clearly reveal capillary condensation accompanied by a very wide hysteresis loop (see Figures 2a, 3a, and 4a). Figure 2b shows that argon (at 87.3 K) fills the micropores in SE3030 at a higher relative pressure as compared to nitrogen. The adsorption isotherms and the observed characteristic hysteresis loops are reproducible as seen from Figures 3a and 4a, which show two independently measured nitrogen adsorption/desorption isotherms on KLE and KLE/IL silica.

The wide hysteresis loops indicate a delay in both condensation and evaporation. Hence, the mesopore size distributions were calculated from the adsorption branches by applying the nitrogen and argon metastable adsorption branch kernels described above. Studies by TEM,[38] SANS,[41] and SAXS suggest that SE3030 silica consists of wormlike mesopores connected by cylindrical micropores; hence, a cylindrical pore model was assumed for the NLDFT pore size analysis over the complete micro- and mesopore size range. In the case of KLE silica, a cylindrical pore model was assumed for the micropore range, but the mesopore size distribution was calculated on the basis of a spherical pore model,[25a] again, in accordance with the information about the pore structure.[39]

The analysis of the nitrogen and argon adsorption data obtained at 77.4 and 87.3 K, respectively, supports the existence of both micro- and mesoporosity in SE3030 silica. The NLDFT PSD curves for SE3030 show two maxima centered at pore diameters of ca. 10−13 and 90−95 Å (see Figure 2d). The mesopore size distributions calculated from nitrogen (77.4 K) and argon (87.3 K) isotherms are in excellent agreement, including cumulative pore volume plots (Figure 2c). Note, that calculations for argon were not extended in the range of micropores. From the nitrogen isotherm, a specific surface area of ca. 600 m^2/g was obtained by formally applying the BET method in the relative pressure range from 0.05 to 0.15 (using a cross-sectional area of 16.2 $Å^2$ for the nitrogen molecule). One should keep in mind that the BET surface area in materials, such as SE3030, which contain a substantial amount of microporosity, does not correlate with the geometrical surface area and can only be considered as a BET equivalent surface area.

Similar to SE3030, KLE silica also contains micropores centered at ca. 13 Å; however, the diameter of spherical mesopores is ca. 139 Å (see Figure 3b) that is significantly larger than the size of the wormlike mesoporous channels in SE3030 silica. The nitrogen equivalent BET surface area is ca. 310 m^2/g.

The NLDFT pore diameters for SE3030 and KLE silicas are in very good agreement with independent pore size data of TEM and SANS/SAXS methods;[38,39] i.e., micropores of diameter ca. 10−13 Å were obtained for both SE3030 and KLE silica (see Tables 1 and 2). The application of TEM and SANS revealed a mesopore size of ca. 95 Å for SE3030.[38,41] In the case of KLE silica, a pore diameter of ca. 138 Å was obtained for the spherical mesopores by SAXS (for details, please see ref 39).

For KLE/IL silica, we obtained a trimodal pore size distribution (Figure 4c). Similarly to KLE silica, some microporosity is revealed; the pore size distribution curve is centered at around

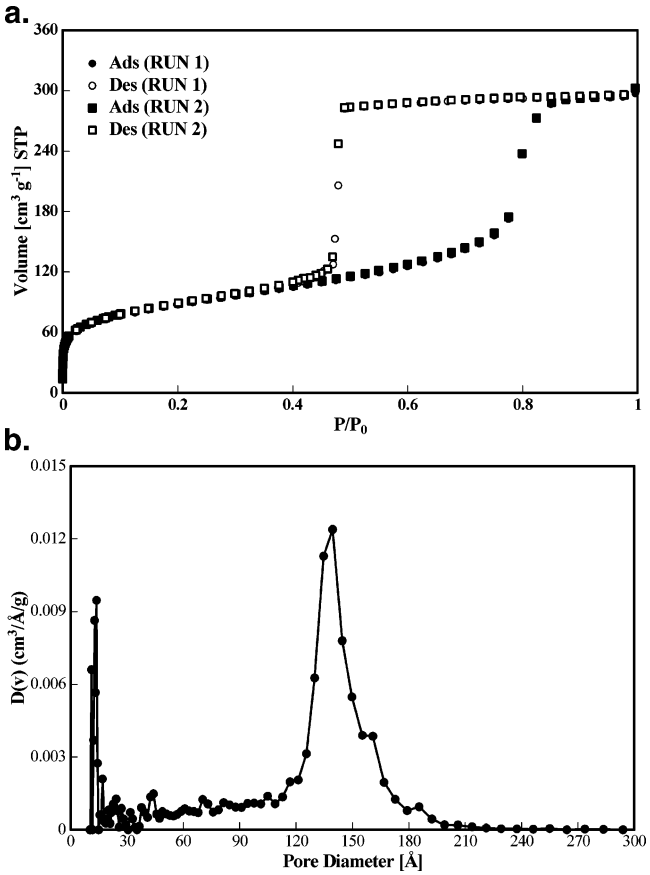

Figure 3. (a) High-resolution nitrogen (77.4 K) adsorption/desorption isotherms on KLE silica. (b) NLDFT pore size distribution for KLE silica calculated from the adsorption branch of the N_2 isotherm shown in a by applying the kernel of metastable adsorption isotherms. The hybrid NLDFT kernel used here is based on a cylindrical pore model for the micropore range and a spherical pore model for the mesopore range in which hysteresis is observed.

13 Å, and the PSD of the large mesoporous cavities (i.e., pore diameter of 139 Å) is also similar to KLE silica. The pore diameter of the narrow mesopores is 26 Å. A BET-equivalent surface area of ca. 700 m^2/g was obtained from the nitrogen isotherm (the BET analysis was performed in the relative pressure range from 0.007 to 0.05).

SAXS data for the sample of KLE/IL silica and a high-resolution TEM image are presented in Figures 5 and 6, respectively. The SAXS data show various interferences, which are attributable to an ordered hierarchical micropore structure. In particular, it is noteworthy that, in contrast to previous publications on similar systems,[42] the packing of the smaller mesopores in the walls between the larger ones was visible in the SAXS data as a broad maximum at around $s = 0.03$ Å^{-1}. A detailed SAXS analysis by applying a Percus Yevick approach (see ref 40) reveals a quite uniform diameter of 137 Å for the spherical cages and 28 Å for the smaller mesopores, while the latter show a significant variance of ca. 2−3 Å based on the SAXS procedure. Nevertheless, also for this material, a very good agreement is obtained with the results of adsorption/NLDFT analysis.

The fact that the mesopore size distributions obtained with the NLDFT adsorption kernels agree so well with SANS and SAXS data confirms the validity of the NLDFT method for the pore size analysis of micro- and mesoporous materials.

(42) Groenewolt, M.; Antonietti, M.; Polarz, S. *Langmuir* **2004**, *20*, 7811.

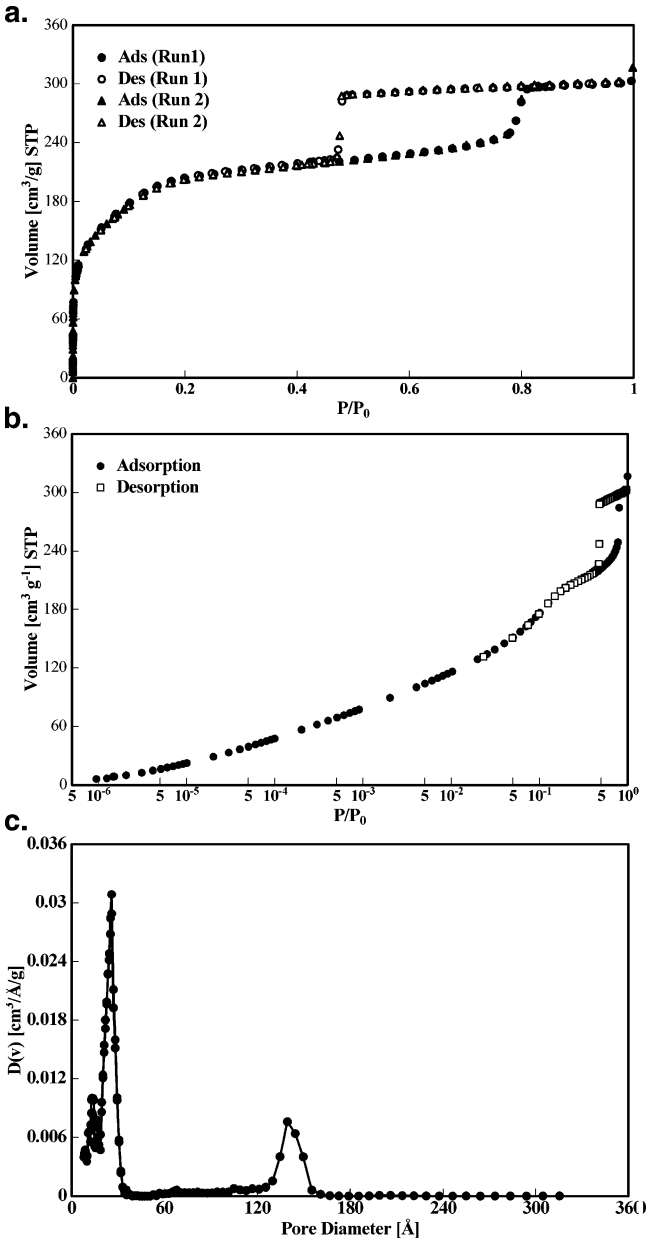

Figure 4. (a) High-resolution nitrogen (77.4 K) adsorption/desorption isotherms on KLE/IL silica. (b) Semilogarithmic plot of a nitrogen (77.4 K) isotherm on KLE/IL silica measured over a relative pressure range from 10^{-6} to 1. (c) NLDFT pore size distribution for KLE/IL silica calculated from the adsorption branch by applying the kernel of metastable adsorption isotherms on the adsorption data shown in b. The hybrid NLDFT kernel used here is based on a cylindrical pore model for the micropore and narrow mesopore (pore diameter <5 nm) range and a spherical pore model for the mesopore range in which hysteresis is observed.

3.2. Mechanism of Pore Evaporation in Micro- and Mesoporous Materials: Pore Blocking or Cavitation? Adsorption data on KLE/IL silica clearly demonstrate a cavitation-controlled mechanism of evaporation. Indeed, this material presents an example of well-defined ink-bottle pores with a quite uniform neck diameter of 26 Å, which was established by adsorption and SAXS techniques. This result is in agreement with NLDFT calculations[25] and earlier experiments,[25b] which showed that desorption occurs via cavitation for neck diameters smaller than 40−50 Å. The nitrogen adsorption isotherm on KLE/IL silica clearly demonstrates that, even though the fluid evaporates from the pore body in the process of cavitation, the

Table 1. Surface and Pore Size Characterization of SE3030 Silica by Nitrogen Adsorption, SANS, and TEM Analysis

	SE3030 silica
S_{BET} (N_2) (m^2/g) with $\alpha_{sx} = 16.2$ Å^2	600 ($P/P_0 = 0.05-0.15$)
S_{SANS} (m^2/g)	550[38]
total (Gurvich) pore volume at ($P/P_0 = 0.95$) (cm^3/g)	0.70
NLDFT micropore volume (cm^3/g)	0.11
SANS micropore volume (cm^3/g)	0.1[38,41]
NLDFT mesopore volume (cm^3/g)	0.58
NLDFT micropore diameter (Å)	11
SANS micropore diameter (Å)	10[41]
NLDFT mesopore diameter (Å)	94 (from N_2,77.4 K); 91 (from Ar, 87.3 K)
SANS mesopore diameter (Å)	ca. 95[41]
TEM mesopore diameter (Å)	ca. 95[38]

Table 2. Surface Area and Pore Size Characterization of KLE Silica and KLE/IL Silica by Nitrogen Adsorption, SAXS, and TEM Analysis

	KLE silica	KLE/IL silica
S_{BET} (m^2/g) with $\alpha_{sx} = 16.2$ Å^2	310 ($P/P_0 = 0.05-0.2$)	670 ($P/P_0 = 0.007-0.05$)
total (Gurvich) pore volume at ($P/P_0 = 0.95$) (cm^3/g)	0.46	0.47
NLDFT pore volume (for pores <300 Å) (cm^3/g)	0.44	0.44
NLDFT micropore diameter (Å)	13	13
NLDFT mesopore diameter (Å)	139	bimodal mesopore size distribution, modes at 26 and 139
SAXS mesopore diameter (Å)	138[39]	28 and 137
TEM mesopore diameter (Å)	ca. 130[39]	ca. 135

constrictions (necks) remain filled until a significantly lower relative pressure is reached (Figure 4a). Both filling and desorption from the necks are reversible processes.

In general, the hysteresis loops observed in micro- and mesoporous materials can be affected by both percolation and cavitation mechanisms. The pore size distribution of mesopores can be calculated, as demonstrated in the previous section, from the adsorption branch of the isotherm by applying a proper NLDFT method. However, as discussed in the Introduction, one can potentially obtain information about the neck sizes directly from the desorption branch, but only if the percolation is the dominating mechanism of pore evaporation. Hence, it is important to determine which of the mechanisms controls the position of the desorption branch.

As a simple test to detect the mechanism of evaporation, we propose to measure the adsorption isotherms of different adsorptives (i.e., simple fluids such as argon and nitrogen) in combination with a proper method for the calculation of the pore size distribution. If percolation is a dominant mechanism, the evaporation pressure is controlled by the size of the necks (or the connecting pores). Hence, the "pore size distribution" calculated from the desorption branch should be independent of the choice of the adsorptive and temperature; i.e., one would expect to find a good agreement between the pores size distribution curves obtained from different adsorptives. In contrast, if evaporation occurs by cavitation, the position of the evaporation step is not correlated with the neck size. In such a case, an artificial "pore size distribution" determined from the desorption branch should depend upon the choice of the adsorptive; i.e., the PSD results calculated from the desorption branches of isotherms of different adsorptives should be substantially different.

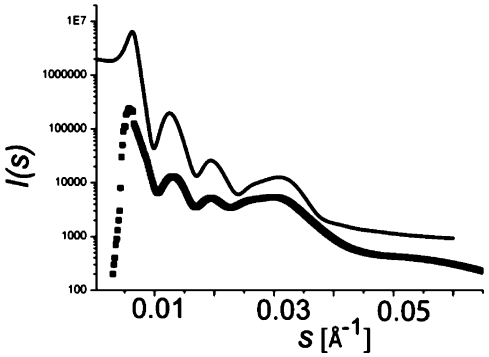

Figure 5. SAXS curve of KLE/IL silica (■) and fitting (●).

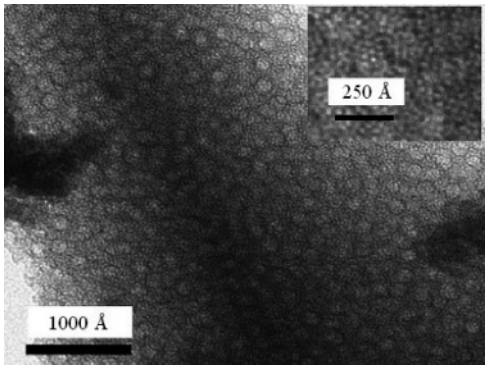

Figure 6. TEM image of KLE/IL silica. The inset is the high-magnification SEM image.

This simple test was applied to SE3030 silica and Vycor glass. Figure 7a shows adsorption isotherms of argon (at 87.27 K) and nitrogen (at 77.35 K) on Vycor glass. For both gases, the adsorption isotherms feature a characteristic type H2 hysteresis loop. The NLDFT pore size distribution obtained from the adsorption branches of nitrogen and argon isotherms are in good agreement (see Figure 7b). We find also a perfect agreement for the PSD curves obtained from the desorption branches (see Figure 7c). Hence, this example clearly indicates that the percolation mechanism is in effect for Vycor glass. Information about the size of narrow mesopore channels ("necks") connecting larger mesopores can be obtained from the desorption branch. However, the width of the pore size distribution obtained from the desorption branch is still artificially narrow because the liquid evaporates from both the constrictions and the larger pores simultaneously. On the contrary, the adsorption branch contains information about the size of pore bodies, and the width of the calculated pore size distribution looks more realistic.

A different result is observed for SE3030 silica. While the NLDFT pore size distributions obtained from the adsorption branches of nitrogen (77.4 K) and argon (87.3K) isotherms are in excellent agreement (parts c and d of Figure 2), the pore size distributions calculated from the desorption branches of nitrogen and argon isotherms are drastically different, which confirms the cavitation-controlled mechanism of evaporation in SE3030 silica (see Figure 8). It should be noted that this result contradicts the conclusions of ref 38, in which the wide hysteresis loop for SE3030 silica was attributed to pore-blocking effects.

3.3. Effect of Pore Structure and Temperature on Cavitation. The question of whether the pore shape and size, and also the size of pore necks affect the cavitation pressure can be discussed by comparing the adsorption behavior of nitrogen and argon in SE3030, KLE, and KLE/IL silicas. Figure 9 shows nitrogen adsorption isotherms on SE3030 and KLE/IL silicas. The two materials differ in the shape and size of mesopores

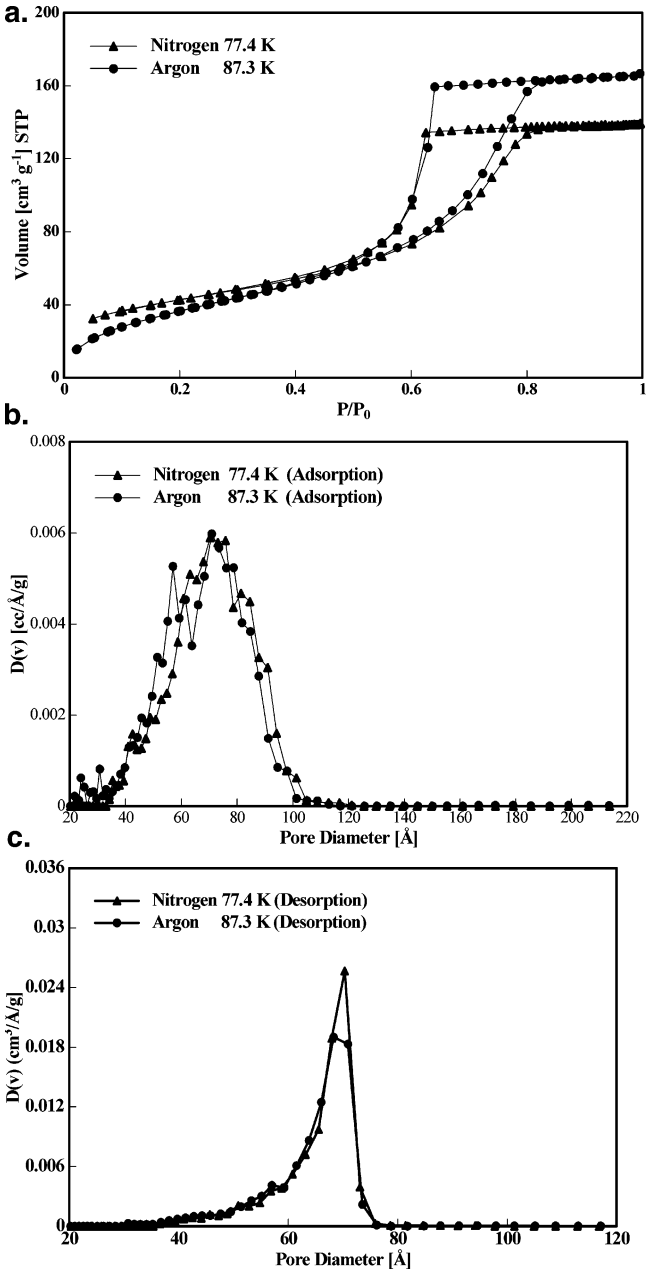

Figure 7. (a) Nitrogen (77.4 K) and argon (87.3 K) adsorption/desorption on porous Vycor glass. (b) NLDFT pore size distribution curves for Vycor calculated from the adsorption branch of the sorption data shown in a by applying the kernels of metastable adsorption isotherms based on a cylindrical pore model for the systems nitrogen (77.4 K)/silica and argon (87.3 K)/silica. (c) NLDFT pore size distribution curves for Vycor glass obtained from the desorption branches of the sorption data shown in a by applying the NLDFT equilibrium transition kernel (on the basis of a cylindrical pore model) for the systems nitrogen (77.4 K)/silica and argon (87.3 K)/silica.

(wormlike cylindrical mesopores of pore diameter ~ 95 Å) in SE3030 versus spherical mesopores (pore diameter ~ 139 Å in KLE/IL), as well as in size of the connecting pores. Figure 10a shows nitrogen adsorption isotherms at 77.4 K on KLE and KLE/IL silicas. These materials contain spherical cavities with a pore size distribution centered at around 139 Å, but they differ appreciably with regard to the size of the connecting pores. The cumulative and differential pore volume distributions in KLE and KLE/IL silicas (see parts b and c of Figure 10) reveal microporosity in the pore walls. In addition, KLE/IL silica contains a substantial amount of small 26 Å mesopores (ca. 0.25 cm^3/g).

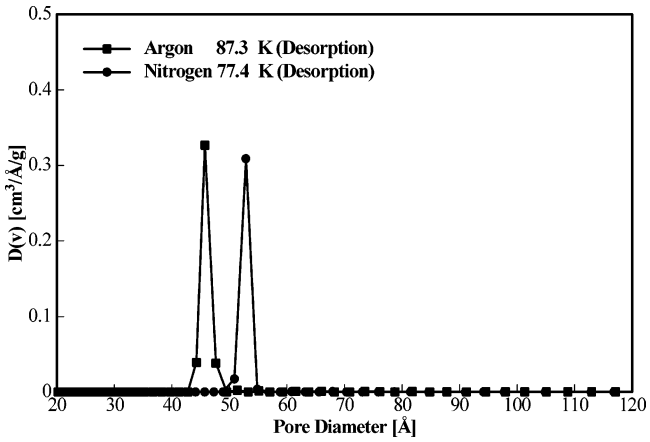

Figure 8. NLDFT pore size distribution curves for SE3030 silica obtained from the desorption branch of the adsorption/desorption data shown in Figure 2b by applying the NLDFT equilibrium transition kernel (on the basis of a cylindrical pore model) for the systems nitrogen (77.4 K)/silica and argon (87.3 K)/silica.

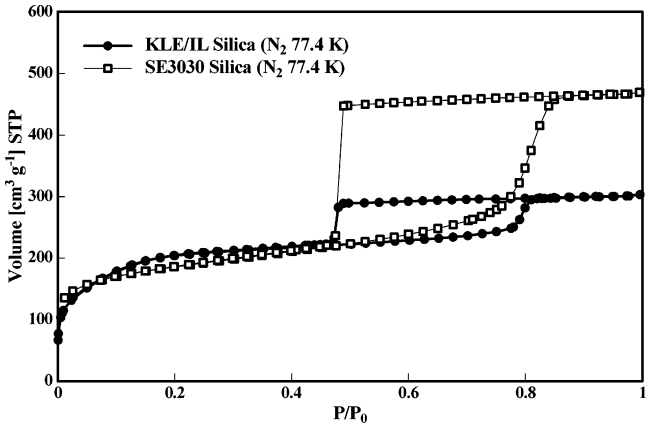

Figure 9. Comparison of the adsorption/desorption behavior of nitrogen (at 77.4 K) in SE3030 and KLE/IL silica.

This means that in KLE silica the cavities are connected through the network of micropores, while in KLE/IL, they are also connected by small mesopores.

Despite the prominent differences in pore structure, the cavitation-controlled evaporation occurs, in all of the materials considered in this work, within a very narrow range of relative pressures between the onset of cavitation and the closure point of the hysteresis loop, which are clearly defined on the stepwise desorption isotherm (from $P/P_0 \sim 0.49$ to ~ 0.47 for nitrogen at 77.4 K). Similar cavitation behavior was found in FDU-1 and SBA-16 silicas with spheroidal cavities of diameters 85 and 150 Å, respectively.[25] This means that the cavitation in pores wider than 85 Å does not depend upon the pore shape and size and also on the size of connecting pores (at least for the pore necks smaller tha 26 Å) appreciably.

It is further interesting to note that in KLE silica (see Figures 3 and 10a), the desorption branch consists of two regions; i.e., the main part reflects the cavitation transition (at the relative pressures of 0.49−0.47 for nitrogen at 77.4 K, 0.32−0.30 for argon at 77.4 K, and 0.45−0.43 for argon at 87.3 K), and a small "tail", which leads to a closure of the hysteresis loop at smaller relative pressures, i.e., about 0.42 for nitrogen at 77.4 K, about 0.25 for argon at 77.4 K, and about 0.38 for argon at 87.3 K. The origin of this "tail" is not completely understood, but the lower closure point of the hysteresis loop agrees with the "universal" limit of hysteresis observed in cylindrical pores of MCM-41.[25] A possible explanation is that KLE silica contains

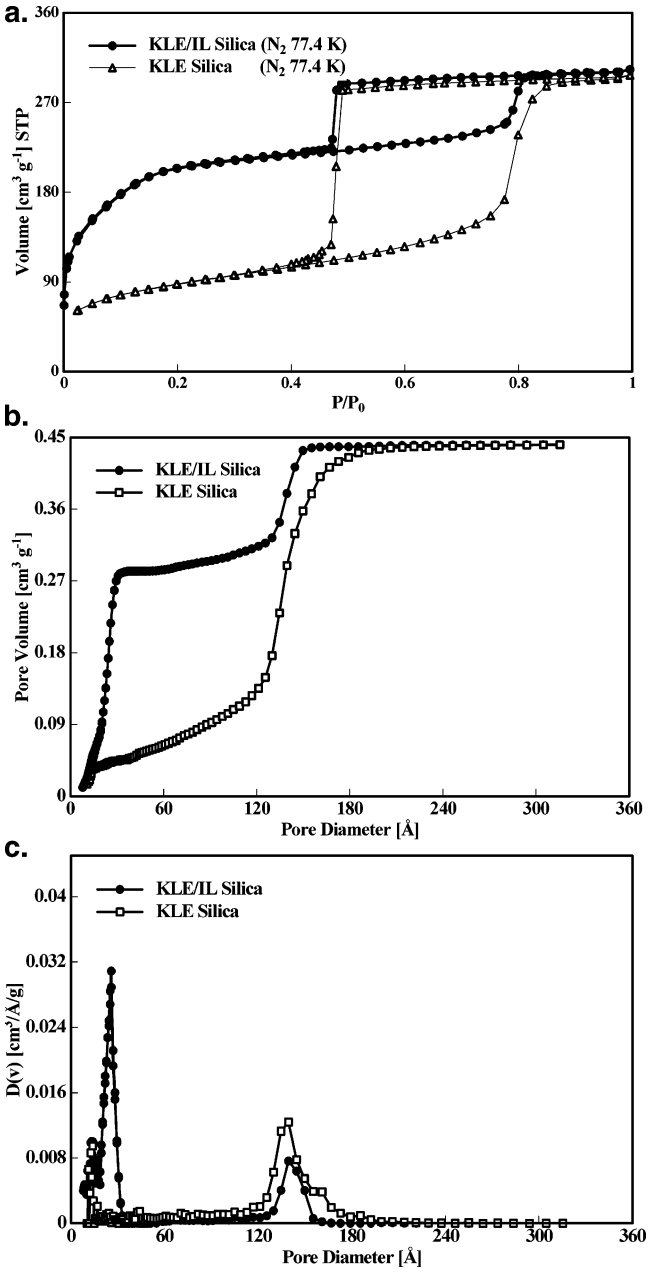

Figure 10. (a) Comparison of adsorption/desorption behavior of nitrogen (at 77.4 K) in KLE silica and KLE/IL silica. (b) Comparison of NLDFT cumulative pore volume for KLE silica and KLE/IL silica. (c) Comparison of NLDFT differential pore size distributions for KLE silica and KLE/IL silica.

a small fraction of irregular mesopores of a somewhat smaller size than the main cagelike mesopores.

The effect of temperature on cavitation is significant. This is clearly seen in Figure 11 with adsorption isotherms of argon in KLE/IL silica at 87.3 and 77.4 K (the adsorption isotherm at 77.35 K is plotted by using the saturation pressure of supercooled liquid, i.e., $P_0 = 230$ Torr[43]). Figure 11 shows that as the temperature decreases, the condensation pressure and cavitation pressure decrease. The cavitation at 87.3 K occurs at $P/P_0 = 0.44-0.43$, whereas at 77.4 K, it occurs at $P/P_0 = 0.31-0.30$.

4. Conclusions

We performed systematic nitrogen and argon adsorption studies of micro- and mesoporous materials with four distinctly different pore structures: (1) micro- and mesoporous SE3030 silica with wormlike randomly blocked channels, (2) micro- and mesoporous KLE silica with an array of spherical mesopores, (3) trimodal KLE/IL silica with micropores and cylindrical, and spherical mesopores, and (4) Vycor glass with a disordered network of mesopores. The structure of silica materials had been previously characterized by TEM, SANS, and SAXS studies.[38−41]

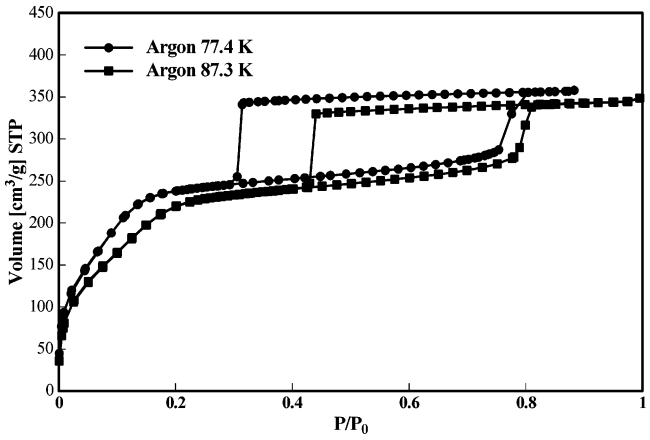

Figure 11. Effect of temperature on the cavitation transition of argon at 77.4 and 87.3 K in KLE/IL silica (please note that the adsorption/desorption isotherm at 77.35 K is plotted by using the saturation pressure of supercooled liquid, $P_0 = 230$ Torr). At 87.3 K, cavitation starts at a relative pressure of ca. 0.44, whereas at 77.4 K, the onset of cavitation can be observed at a relative pressure of 0.31.

We developed a new hybrid NLDFT method to calculate pore size distributions in materials containing pores of different geometry. The pore size distributions calculated by the NLDFT method are in agreement with the results obtained from independent SANS/SAXS methods. In SE3030 silica, we found that the average size of mesopores is ∼95 Å as obtained by the NLDFT method using the cylindrical pore model and by SANS using the hard-disk model of Rosenfeld. Moreover, micropores with an average size of 10−13 Å and a broad distribution have been assessed by both methods. In KLE silica, we found ∼139 Å mesopores from the NLDFT method using a spherical pore model, which agrees well with the SAXS pore diameter of ∼138 Å calculated by using the Percus−Yevick approach. Finally, in the trimodal KLE/IL silica, we found ∼139 Å spherical and ∼26 Å cylindrical mesopores from adsorption compared to ∼137 and 28 Å SAXS diameters, respectively.

We confirmed our previous conclusions regarding the mechanisms of hysteresis in ink-bottle-type pores.[25] We further demonstrated that adsorption measurements with different adsorptives allows one to identify and separate the effects of pore-blocking and cavitation-controlled evaporation (desorption). The results show that cavitation is the dominant mechanism of desorption in SE3030, KLE, and KLE/IL silicas. In this case, the pore size distributions cannot be obtained from an analysis of the desorption branch of the isotherm. An example of KLE/IL silica clearly shows that desorption in the structure consisting of large mesopores connected by smaller mesopores occurs first by cavitation of the liquid in the large mesopores followed by the desorption from smaller mesopores. In contrast, we confirmed that the percolation effects, rather than cavitation, contribute into the hysteresis observed in Vycor glass. In this case, information about the size of the pore necks can be obtained from the desorption branch.

(43) Neimark, A. V.; Ravikovitch, P. I.; Grün, M.; Schüth, F.; Unger, K. K. *J. Colloid Interface Sci.* **1998**, *207*, 159.

Our results reveal that the cavitation pressures of nitrogen at 77.4 K and argon at 77.4 and 87.3 K in SE3030, KLE, and KLE/IL silicas do not depend upon the pore shape and size appreciably. They are noticeably higher (ca. $0.05-0.06P_0$) than the lower limit of hysteresis in MCM-41 materials containing an array of cylindrical pores. These observations are in agreement with our previous results for FDU-1 and SBA-16 silicas.[25b] That is, no appreciable confinement effect on the bubble nucleation is observed in the materials with large mesopores (pore diameters > 85 Å) considered in this paper and in ref 25. However, our ongoing measurements show a slight yet detectable decrease of the cavitation pressure as the pore size decreases. This conclusion agrees with the correlation between the desorption and adsorption pressures in the cagelike materials presented in ref 31.

Acknowledgment. The work was supported by the TRI/Princeton exploratory research program and Quantachrome Instruments. A part of this research was performed at Princeton University, where one of us (A.V.N.) worked in 2004−2005 as a Guggenheim Fellow. A.V.N. gratefully acknowledges the support of the John Simon Guggenheim Memorial Foundation and thanks George Scherer for his hospitality and fruitful discussions. B.S. gratefully acknowledges the Max-Planck Society for financial support, Prof. M. Antonietti for scientific discussions, and Dr. E. Hoinkis (Hahn-Meitner Institute, Berlin, Germany) for help with the SANS-sorption measurements.

LA051686H